AGU PUBLICATIONS

JGR

Journal of Geophysical Research: Space Physics

RESEARCH ARTICLE
10.1002/2017JA024723

Properties of the Equatorial Magnetotail Flanks ~50–200 R_E Downtail

A. V. Artemyev[1,2], V. Angelopoulos[1], A. Runov[1], C.-P. Wang[3], and L. M. Zelenyi[2]

[1]Institute of Geophysics and Planetary Physics, University of California, Los Angeles, CA, USA, [2]Space Research Institute, RAS, Moscow, Russia, [3]Department of Atmospheric and Oceanic Sciences, University of California, Los Angeles, CA, USA

Key Points:
- Dynamical pressure does not contribute to pressure balance across the equatorial magnetotail boundary at lunar orbit and farther downtail 200 R_E
- High-beta plasmas without a significant magnetic field pressure are observed
- Total energies (kinetic plus thermal) are very close for the plasma sheet and magnetosheath ions

Correspondence to:
A. V. Artemyev,
aartemyev@igpp.ucla.edu

Citation:
Artemyev, A. V., Angelopoulos, V., Runov, A., Wang, C.-P., & Zelenyi, L. M. (2017). Properties of the quatorial magnetotail flanks ~50–200 R_E downtail. *Journal of Geophysical Research: Space Physics*, *122*. https://doi.org/10.1002/2017JA024723

Received 29 AUG 2017
Accepted 4 NOV 2017
Accepted article online 9 NOV 2017

Abstract In space, thin boundaries separating plasmas with different properties serve as a free energy source for various plasma instabilities and determine the global dynamics of large-scale systems. In planetary magnetopauses and shock waves, classical examples of such boundaries, the magnetic field makes a significant contribution to the pressure balance and plasma dynamics. The configuration and properties of such boundaries have been well investigated and modeled. However, much less is known about boundaries that form between demagnetized plasmas where the magnetic field is not important for pressure balance. The most accessible example of such a plasma boundary is the equatorial boundary layer of the Earth's distant magnetotail. Rather, limited measurements since its first encounter in the late 1970s by the International Sun-Earth Explorer-3 spacecraft revealed the basic properties of this boundary, but its statistical properties and structure have not been studied to date. In this study, we use Geotail and Acceleration, Reconnection, Turbulence and Electrodynamics of the Moon's Interaction with the Sun (ARTEMIS) missions to investigate the equatorial boundary layer from lunar orbit (~55 Earth radii, R_E, downtail) to as far downtail as ~200 R_E. Although the magnetic field has almost no effect on the structure of the boundary layer, the layer separates well the hot, rarefied plasma sheet from dense cold magnetosheath plasmas. We suggest that the most important role in plasma separation is played by polarization electric fields, which modify the efficiency of magnetosheath ion penetration into the plasma sheet. We also show that the total energies (bulk flow plus thermal) of plasma sheet ions and magnetosheath ions are very similar; that is, magnetosheath ion thermalization (e.g., via ion scattering by magnetic field fluctuations) is sufficient to produce hot plasma sheet ions without any additional acceleration.

1. Introduction

Earth's magnetosphere, a region bounded by the magnetopause and topologically connected to the planet is populated by ionospheric and solar wind plasmas. The simplest way for shocked solar wind plasma to travel from interplanetary magnetic field lines to closed magnetosphere field lines is by reconnection, which occurs at the dayside and nightside (cusp) magnetopause (depending on the interplanetary magnetic field orientation) as well as in the distant magnetotail (Dungey, 1963). Because this transport mechanism does not account for all the plasma observed to enter the magnetosphere, several alternative mechanisms have been considered to describe plasma transport across the magnetopause (see review by Wing et al., 2014, and references therein).

Strong plasma pressure and magnetic field gradients at the magnetopause serve as a free energy source for various plasma waves that enable stochastic charged particle diffusion across the magnetic surfaces (e.g., Chen et al., 2015; Galeev et al., 1986; Johnson & Cheng, 1997; Treumann, 1999, and references therein). The stochastic transport can be enhanced by large-scale magnetopause perturbations as Kelvin-Helmholtz vortexes (e.g., Chen et al., 2015; Fairfield et al., 2000; Hasegawa et al., 2004; Nakai & Ueno, 2011) or as various surface waves (e.g., De Keyser & Roth, 2003; Plaschke, 2016; Sibeck et al., 1990) usually observed at the flanks of the magnetosphere. Such plasma transport results in formation of a boundary layer with a monotonic, gradual plasma density profile (e.g., De Keyser et al., 2004; Fujimoto et al., 1997, 1998; Phan, 1997). Investigation of the structure and dynamics of the magnetopause and its boundary layer at different locations plays an important role for understanding transport of particles, momentum, and energy from the solar wind into the magnetosphere.

The dayside (and near-Earth nightside) magnetopause is a tangential discontinuity (e.g., De Keyser et al., 2005; Sanchez et al., 1990) in which intense currents are consistent with strong magnetic field gradients (e.g., Haaland et al., 2014; Panov et al., 2008; Šafránková et al., 2007) that separate magnetosheath plasmas from magnetosphere plasmas. In the absence of a magnetic field (normal to the magnetopause), generated by reconnection or by plasma waves, magnetized magnetosheath plasma cannot cross such strong magnetic fields to enter the magnetosphere. The decrease in magnetic field intensity with distance from Earth leads to significant variations of the magnetospheric boundary's properties. Data collected by ISEE-3 (Ogilvie et al., 1977) and Geotail (Nishida, 1994) beyond lunar orbit demonstrated that magnetosheath plasma may move through the distant magnetopause much more easily than through the near-Earth magnetopause. First, the high-latitude distant magnetopause is often a rotational discontinuity open for plasma transport into the magnetosphere's lobes (Hasegawa et al., 2002). (This plasma, which populates almost empty magnetic field lines at high latitudes, can be detected by spacecraft only via electric drift instruments (e.g., Haaland et al., 2008).) Second, the flank distant magnetopause structure, which depends essentially on interplanetary magnetic field orientation (e.g., Hasegawa et al., 2000; Sibeck & Lin, 2014; Sibeck, Siscoe, Slavin, Smith, Tsurutani, & Lepping, 1985), is often open for plasma entry into the magnetosphere (Grzedzielski & Macek, 1988; Sibeck, Siscoe, Slavin, Smith, & Tsurutani, 1985; Wang, Lyons, et al., 2014). Large-scale numerical simulations of test particles in MHD fields support the idea of plasma transport into the magnetosphere through the distant flank magnetopause (e.g., Peroomian, 2003; Peroomian & El-Alaoui, 2008). However, unlike the structure of the near-Earth magnetopause and boundary layer, which have been intensively investigated by Cluster and Time History of Events and Macroscale Interactions during Substorms (THEMIS) missions, that of the distant magnetopause remains poorly studied observationally.

Modeling of plasma transport mechanisms and their efficiency in the distant magnetopause require investigation of its kinetic structure. Observations at lunar orbit (around −55 Earth radii, R_E, downtail) clearly show the presence of a boundary layer separating cold, flowing magnetosheath plasmas from hot, stagnant, plasma sheet plasmas (e.g., Chen et al., 2015; Wang, Xing, et al., 2014). Weak magnetic fields at the low-latitude magnetotail flanks (plasma sheet flanks) suggest that the nightside magnetopause configuration should differ significantly from the dayside configuration (e.g., Panov et al., 2008; Phan & Paschmann, 1996) and from the configuration of the near-Earth flank (e.g., Haaland et al., 2014; Sanchez et al., 1990), where the magnetic field plays the most important role in the pressure balance (De Keyser et al., 2005). In the absence of a strong magnetic field, separation of different plasmas should be supported by other mechanisms. In this study, we investigate the mechanisms responsible for formation of the distant magnetopause and the equatorial boundary layer. We use Acceleration, Reconnection, Turbulence and Electrodynamics of the Moon's Interaction with the Sun (ARTEMIS) (Angelopoulos, 2011) observations from as close as lunar orbit (~55 R_E) to as far downtail as 200 R_E and Geotail (Nishida, 1994) observations over similar radial distances. From plasma characteristics, we construct a simple kinetic model of the low-latitude distant boundary layer and explain the plasma dynamics near this magnetosphere boundary.

2. Data Sets

In this study we use three data sets. The first includes 13 ARTEMIS P2 crossings of the boundary layer in 2010, when this spacecraft visited the distant magnetotail ($r \sim 50–200\ R_E$ downtail). The second includes 49 ARTEMIS P2 crossings of the boundary layer in 2011 and 2012 from around lunar orbit ($r \sim 55\ R_E$). The third includes 11 Geotail crossings of the boundary layer in 1994 from two orbits in the distant tail ($r \sim 50–100\ R_E$). The largest data set is the second one, which describes boundary layer properties at lunar distances. The first data set shows that the more distant boundary layer has a structure and properties similar to those of the lunar distant boundary layer. The Geotail data set is used for independent cross checking of the boundary layer properties collected by ARTEMIS.

We use the electrostatic analyzer on board ARTEMIS (McFadden et al., 2008), which collects ion and electron distributions for particles with energies below ~25 keV; ion and electron pressure p_i, p_e (components transverse to the magnetic field); ion and electron bulk velocities $\mathbf{v}_i$, $\mathbf{v}_e$; and electron density n_e (assuming the quasi-neutrality). We also use magnetic field **B** measured by the fluxgate magnetometer (Auster et al., 2008). The time resolution of plasma data collected by ARTEMIS P2 in lunar orbit (the second data set) is 3–4 s (spin resolution). Data collected by ARTEMIS P2 in the distant tail (the first data set) have a time resolution of ~1 min.

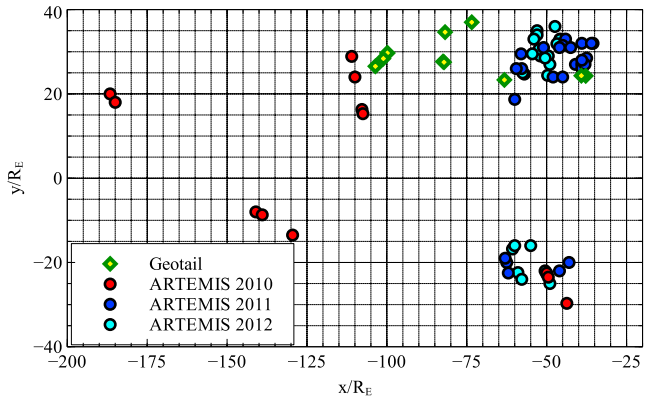

Figure 1. Distribution of events from three data sets in the GSM (x, y) plane.

We use ion pressure, density, and bulk velocity measured by the low-energy particle experiment (Mukai et al., 1994) and magnetic field measured by the magnetic field experiment (Kokubun et al., 1994). The time resolution of plasma measurements on board Geotail is 12 s.

Figure 1 shows the distribution of events from three data sets in the (x, y) plane (GSM coordinates are used through this study). Although most events are in the dusk flank ($y > 0$), several are in the dawn flank ($y < 0$).

Each event represents a full crossing of the boundary layer in the equatorial magnetotail flank. Figure 2 presents two events from the first data set (ARTEMIS P2, 2010). The top panels show the variation of ion and electron bulk velocities v_x across the boundary layer. The plasma sheet side is characterized by low v_x, low-density n_e, and a broad energy distribution (see bottom panels). The ion thermal energy (temperature) significantly exceeds the ion kinetic energy $m_p v_{xi}^2/2$ (m_p is the proton mass) on the plasma sheet side. The magnetosheath side is characterized by strong, dense plasma flow with the kinetic energy exceeding the thermal energy (see the narrow phase space density peak in the bottom panel). The sum of the plasma and magnetic field pressures is almost constant across the boundary layer: hot, rarefied plasma sheet plasma balances cold, dense magnetosheath plasma. The electron contribution to the pressure is small on both the plasma sheet and magnetosheath sides. The transition region (layer) is characterized by a mixture of cold flowing plasma and hot stagnant plasma. This layer is crossed within a few minutes. Interestingly, both the plasma sheet and magnetosheath sides are characterized by large plasma beta $\beta = 2\mu_0(p_i + p_e)/B^2 > 1$; that is, the magnetic field contribution to the pressure balance is not important. Although the plasma sheet density, n_e, is much lower than that in the magnetosheath, it is still very high for the distant magnetotail (compare the observed $n_e \geq 0.5$ cm^{-3} with $n_e \sim 0.1$ cm^{-3} found for the middle tail at $r > 50\ R_E$ in Artemyev et al., 2017). This is a result of the magnetosheath plasma entry to the magnetotail; that is, the plasma sheet flanks in the distant tail are usually much denser than the middle tail (e.g., Hietala et al., 2017; Vasko et al., 2015).

We compare ARTEMIS 2010 measurements with Geotail measurements collected in 1994 when Geotail was traveling in the distant magnetotail. Figure 3 shows two examples of Geotail boundary layer crossings at $r \sim 100\ R_E$. The top panels show a clear variation of the ion bulk velocity v_x from small positive values on the plasma sheet side to large negative values on the magnetosheath side. Ion phase space density spectrograms reveal very different distributions on these two sides: hot, rarefied plasma in the plasma sheet and dense, cold, flowing plasma in the magnetosheath. The ion pressure is almost constant across the boundary

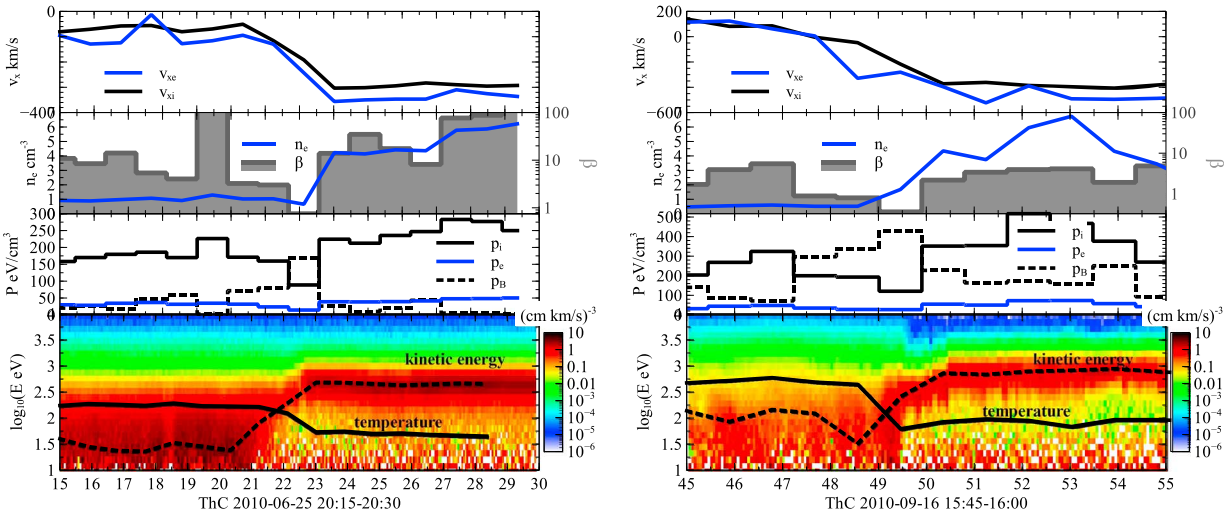

Figure 2. Two ARTEMIS P2 boundary layer crossing events in 2010. From top to bottom: ion and electron velocity v_x, electron density n_e and plasma β, plasma and magnetic field pressures, and phase space density energy-time spectrogram (omnidirectional) with ion temperature and kinetic energy shown by black curves. (left column) The crossing at $x \sim -175\ R_E$, $y \sim 29\ R_E$ and (right column) the crossing at $x \sim -107\ R_E$, $y \sim 16\ R_E$.

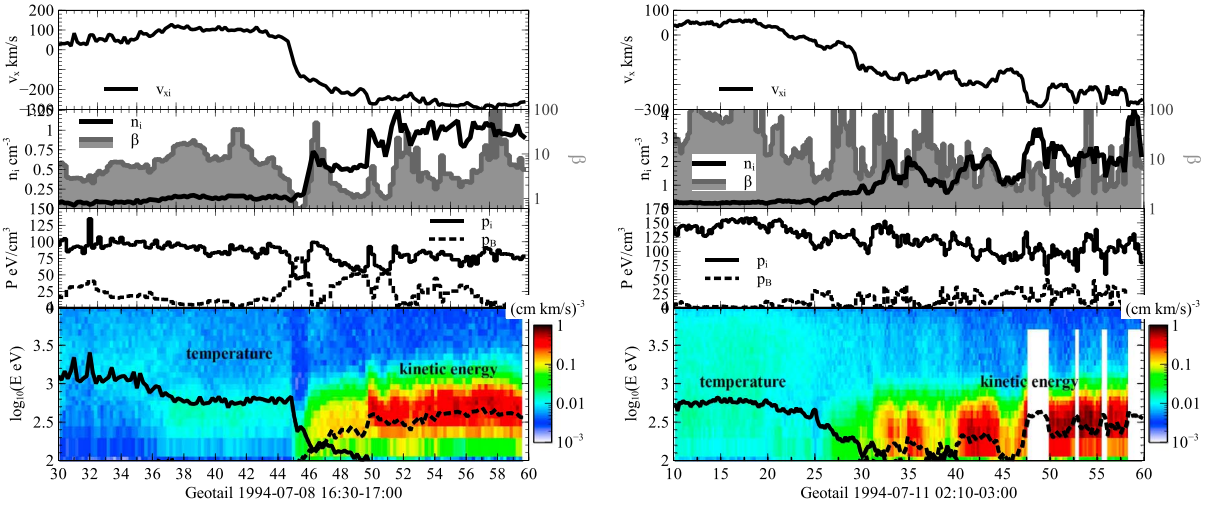

Figure 3. Two boundary layer crossing events observed by Geotail in 1994. From top to bottom: ion velocity v_x, ion density n_i and plasma β, plasma and magnetic field pressures, phase space density energy-time spectrogram (omnidirectional) with ion temperature and kinetic energy overlayed as black curves. (left column) The crossing at $x \sim -82\ R_E$, $y \sim 34\ R_E$; (right column) the crossing at $x \sim -100\ R_E$, $y \sim 22\ R_E$.

layer and much larger than the magnetic field pressure ($\beta \sim 10$). The ion density varies from $n_i < 0.25$ cm^{-3} on the plasma sheet side to $n_i > 1$ cm^{-3} on the magnetosheath side. Therefore, plasma and magnetic field parameters collected by Geotail at $r \sim 100\ R_E$ are similar to those collected by ARTEMIS at $r > 100\ R_E$.

The large statistics of boundary layer crossings was collected for the third data set because ARTEMIS visited the lunar distant magnetotail regularly (a few days per month). Figure 4 shows two boundary layer crossings of the dawn and dusk flanks at $r \sim 55$–$62\ R_E$. There is no significant difference between plasma parameters collected at lunar orbit (Figure 4) and at $r \sim 200\ R_E$ (Figure 2). The ion phase space density spectrograms show a clear separation between plasma sheet and magnetosheath plasmas. Although the magnetic field pressure does not play an important role in the pressure balance on the plasma sheet side, it is apparently large enough to be significant for the pressure balance in the magnetosheath. Plasma β is generally larger than one. The transition region between the plasma sheet and the magnetosheath, where ion thermal and kinetic energies are comparable, was crossed for several minutes and is characterized by a mixed plasma population in the phase space density spectrograms.

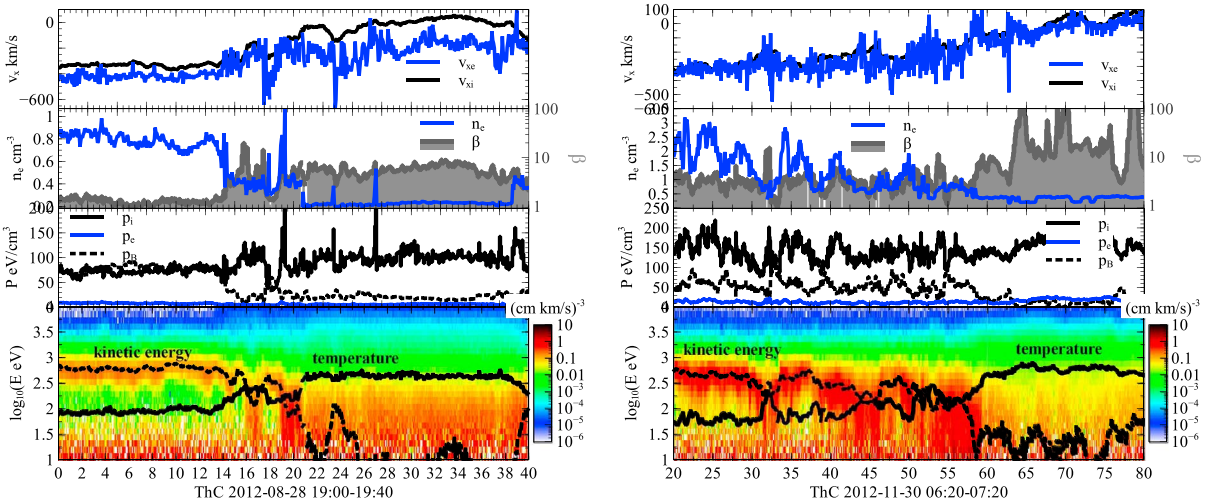

Figure 4. Two ARTEMIS boundary layer crossing events in 2011/2012. From top to bottom: ion and electron velocity v_x, electron density n_e and plasma β, plasma and magnetic field pressures, and phase space density energy-time spectrogram (omnidirectional) with ion temperature and kinetic energy shown by black curves. (left column) The crossing at $x \sim -46\ R_E$, $y \sim 33\ R_E$; (right column) the crossing at $x \sim -59\ R_E$, $y \sim -22\ R_E$.

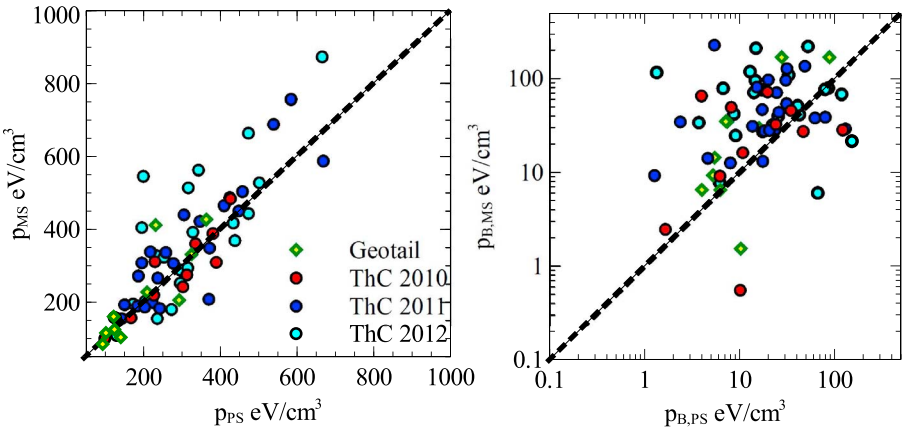

Figure 5. Distribution of the (left) total pressure and the (right) magnetic field pressure in the plasma sheet (PS) and magnetosheath (MS) sides.

Figures 2–4 are typical examples of boundary layer crossing in the middle and distant magnetotails. There is no significant difference between the plasma and the magnetic field around this layer at different distances. Therefore, we combine data collected for the three data sets and analyze them together. To distinguish plasma sheet plasmas from magnetosheath plasmas, we use the following formal criteria: the plasma sheet is characterized by an ion thermal energy 3 times larger than the kinetic energy, whereas the magnetosheath side is characterized by $v_{xi} < -200$ km/s and a kinetic energy 3 times larger than the ion thermal energy. We also visually inspect all events and confirm that the transition region has been excluded from calculation of the statistical properties of the plasma sheet and magnetosheath sides.

3. Statistics of Plasma Parameters Around the Boundary Layer

We start our statistical investigation of boundary layer properties by examining the pressure balance. For each event from our data sets we calculate the average plasma pressure (ions plus electrons in ARTEMIS, only ions in Geotail) and the magnetic field pressure in the plasma sheet (PS) and magnetosheath (MS) sides. Figure 5 (left) shows the total pressure (plasma and magnetic field) distribution. There is a quite good balance between plasma sheet and magnetosheath pressures. Interestingly, the absolute values of pressures and the pressure balance do not depend on radial distance; that is, the distribution of points does not differ qualitatively in different data sets. Figure 5 (right), which shows only the magnetic pressures (we recalculate the magnetic field pressure to eV/cm^3), reveals that the magnetic field contributes slightly more to pressure in the magnetosheath than to in the plasma sheet side. However, the absolute values of the magnetic field pressures are much lower than the total pressures (compare left and right panels in Figure 5).

The well-established pressure balance between the plasma sheet and magnetosheath sides (see Figure 5, left) shows that there is likely no contribution to the pressure balance from the ion dynamical pressure $\sim \mathbf{v}_i^2 m_p n_i/2$ (in a agreement with previous study, see Hasegawa et al., 2000). The main ion flow is along the x direction; thus, to exclude the contribution of the dynamical pressure, the boundary layer surface should be parallel to the x axis. The v_{yi} velocity component cannot significantly influence the pressure balance, because the average v_{yi} does not exceed 50 km/s (Dimmock & Nykyri, 2013), contributing a dynamic that is equivalent to a thermal pressure of particles with the energy ~10 eV, much smaller than the typical magnetosheath temperatures.

The dominance of the plasma pressure on both the plasma sheet and magnetosheath sides is confirmed by Figure 6 (left) showing the distribution of plasma β. The plasma sheet β is larger than the magnetosheath β, and both sides have $\beta > 1$: for most events, the plasma sheet $\beta \in [5, 50]$, whereas the magnetosheath $\beta \in [2, 20]$. Therefore, plasma appears to be basically demagnetized (even in the magnetosheath side where the plasma temperature is low).

Figure 6(right) shows the magnetosonic Mach number M (i.e., the square root of the ratio $^2_i m_p/2$ and $B^2/k_B 2\mu_0 + T_i n_i$) calculated for the plasma sheet and magnetosheath sides. The magnetosheath M, always larger than 1, is distributed uniformly within the range $M \in [1, 4]$. Supersonic plasma flows in the magnetosheath (in the already shocked plasma) can be explained by plasma acceleration by the Ampere force of

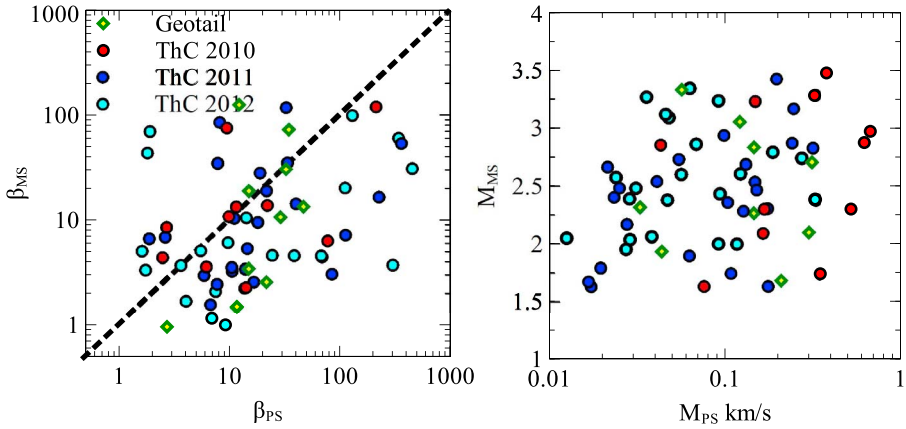

Figure 6. Distribution of (left) β and (right) Mach number in the plasma sheet (PS) and magnetosheath (MS) sides.

draped and curved magnetic field lines in the nightside magnetosheath (e.g., Chen et al., 1993; Erkaev et al., 2011; Harris et al., 2013; Lavraud et al., 2007, and references therein). The plasma sheet M, always less than 1, is distributed within the range $M \in [10^{-2}, 1]$. The fastest plasma flows in the plasma sheet were observed in the distant tail (ARTEMIS 2010 data set) where M can approach 1. Comparison of plasma sheet and magnetosheath Mach numbers shows that this parameter separates well the two plasma populations in the distant magnetotail: as $M_{MS} > 1$ and $M_{PS} < 1$.

Figures 5 and 6 provide the following information about the boundary layer separating plasma sheet plasmas from magnetosheath plasmas: (1) the pressure balance between two plasmas is established mainly by thermal pressure without a significant contribution from dynamic (and magnetic) pressure; (2) plasma β is typically large on both the plasma sheet and magnetosheath sides; that is, the magnetic field pressure is lower than the thermal pressure; and (3) there is the clear separation of plasma characteristics between the plasma sheet and magnetosheath sides: the plasma is stagnant on the plasma sheet side but flows with high velocity (Mach number is large) on the magnetosheath side. Therefore, to describe the observed boundary layer properties, we must explain how the two different plasmas can be separated without strong magnetic fields, which separate plasmas in the dayside or near-Earth magnetopause (e.g., De Keyser et al., 2005; Roth et al., 1996, review, and references therein). To address this problem, we construct an appropriate boundary layer model in the next section.

4. Estimate of Boundary Layer Characteristics

Consider a simple 1-D model of the boundary separating two magnetized plasmas with different properties. The general idea of constructing such a model was proposed by Alpers (1971) and Lemaire and Burlaga (1976) and developed initially for the dayside magnetopause (see, e.g., De Keyser et al., 2013; Lee & Kan, 1979; Roth et al., 1996). However, the main feature of previous magnetopause models is a strong magnetic field contributing to the total pressure; that is, these models describe the magnetopause as a tangential discontinuity (a plasma magnetic field boundary without a magnetic field component normal to the boundary plane). The strong transverse current flowing along the boundary is then responsible for the magnetic field intensity change, whereas field-aligned currents rotate the magnetic field direction (see examples of model-observation comparison in De Keyser & Roth, 1998; Lee & Kan, 1979; Panov et al., 2011). The system's stationarity and the absence of any gradient along the boundary surface provide three integrals of particle motion: the total energy and two generalized momenta. To model the sharp separation between two plasmas, the corresponding distribution function includes a multiplication factor $\sim \mathrm{erf}(A_x)$, where erf is the error function and $A_x(y)$ is the component of the vector potential describing the surface magnetic field variation $B_z(y)$ along the direction normal (y axis) to the boundary surface (see details in the review by Roth et al., 1996).

In the absence of a strong magnetic field, the vector potential cannot be responsible for the separation of the two plasmas. However, this role can be played by the scalar potential $\varphi(y)$ responsible for the polarization field $E_y = -\partial\varphi/\partial y$ directed along the normal to the boundary surface. If we set the scalar potential equal to 0 on the plasma sheet side, it should decrease along y to provide a positive E_y supporting the cross-field ion

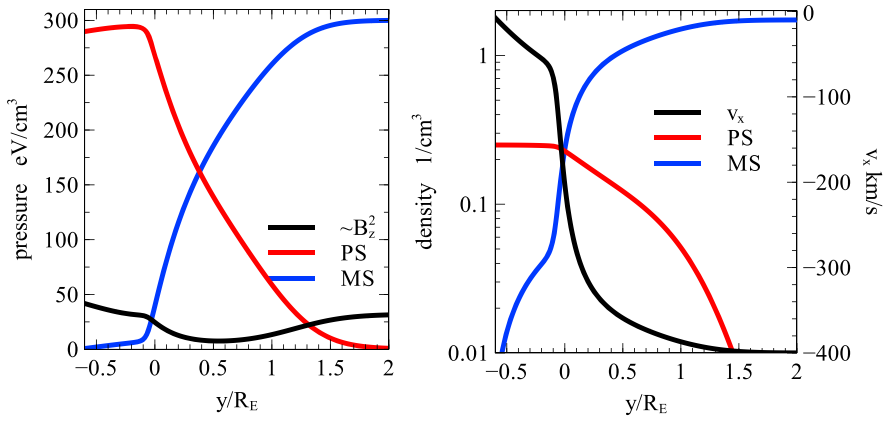

Figure 7. Model distributions of (left) plasma pressure and magnetic field pressure (right) and density and flow velocity for the plasma sheet (PS) and magnetosheath (MS). The magnetic field pressure is shown in Figure 7 (left); the plasma flow velocity is shown in Figure 7 (right). System parameters are $\varphi_0 = 400$ eV, $T_{e,\mathrm{MS}} = 50$ eV, $T_{i,\mathrm{MS}} = 150$ eV, $T_{e,\mathrm{PS}} = 200$ eV, $T_{i,\mathrm{PS}} = 1000$ eV, $u_d = -400$ km/s, and $n_0 = 0.25$ cm^{-3}.

flow $v_x = E_y/B_z$ on the magnetosheath side. Thus, the distribution functions of plasma sheet particles should describe the plasma sheet ion and electron density decrease for $\varphi \to -\infty$, whereas distribution functions of the magnetosheath particles should describe constant ion and electron densities for $\varphi \to -\infty$ and zero densities for $\varphi \to 0$.

There are two methods of constructing plasma equilibrium models. The first method assumes that ion and electron distribution functions f_γ ($\gamma = i$ for ions and $\gamma = e$ for electrons) are introduced as functions of integrals of motion. These integrals depend on scalar φ and vector A_x potentials. Thus, after integrating over velocity space, we obtain particle densities $n_\gamma(\varphi, A_x)$ and currents $j_{x\gamma}(\varphi, A_x)$. The Maxwell equations written through φ, A_x together with $n_\gamma(\varphi, A_x)$, $j_{x\gamma}(\varphi, A_x)$ represent a closed system of equations for φ, A_x (see examples of such magnetopause models in Belmont et al., 2012; Lee & Kan, 1979; Panov et al., 2011; Roth et al., 1996). In 1-D the ion and electron distributions can always be chosen to provide the needed electromagnetic field configuration (Grad, 1961). A second method was proposed by Channell (1976). Ion and electron densities and currents can be chosen as functions of φ, A_x, and the corresponding distribution functions are reconstructed from the solution of the inverse problem (see examples of such solutions in Allanson et al., 2015, 2016). This approach is preferable if we would like to describe the distribution of plasma densities and electric fields of the observed plasma equilibrium, and the information about the particle velocity distributions is less important to us. Therefore, we will use this approach and construct the model with a description of plasma densities for Maxwellian velocity distributions disturbed by strong gradients of the scalar potential φ.

The plasma sheet ion density should contain a multiplication factor describing a Maxwellian energy distribution $n_{i\mathrm{PS}} \sim \exp(-e\varphi/T_{i\mathrm{PS}})$, where e is the unit charge and $T_{i\mathrm{PS}}$ is the plasma sheet ion temperature. To reduce the plasma sheet ion density at on the magnetosheath side, we introduce the multiplication factor $1 + \mathrm{erf}(\varphi/\varphi_0)$, where φ_0 is a typical potential drop across the boundary layer: $n_{i\mathrm{PS}} = n_0 \exp(-e\varphi/T_{i\mathrm{PS}})(1 + \mathrm{erf}(\varphi/\varphi_0))$. This density is constant on the plasma sheet side, where $\varphi \to 0$ but rapidly increases with $\varphi \to -\infty$. The plasma sheet electron density can be introduced as $n_{e\mathrm{PS}} = n_0 \exp(e\varphi/T_{e\mathrm{PS}})$, where $T_{e\mathrm{PS}}$ is the plasma sheet electron temperature. This density approaches n_0 for $\varphi \to 0$ and drops to zero on the magnetosheath side, where $\varphi \to -\infty$. We also take into account a weak dependence of the electron density on A_x to model a weak magnetic field variation caused by electron currents at the boundary layer. This dependence can be included as $n_{e\mathrm{PS}} = n_0 \exp(e\varphi/T_{e\mathrm{PS}} - eu_{d\mathrm{PS}}A_x/T_{e\mathrm{PS}})$, where $u_{d\mathrm{PS}}$ is the plasma sheet electron flow along the boundary surface (such dependence on A_x corresponds to a Maxwellian distribution with a flow velocity $u_{d\mathrm{PS}}$; see Alpers, 1969; Harris, 1962).

The magnetosheath ion and electron densities, $n_{e,i\mathrm{MS}}$, should describe a Maxwellian flowing plasma (both ions and electrons are flowing along the boundary surface at high-velocity u_d): $n_{e,i\mathrm{MS}} = n_0\delta \exp(\mp e\varphi/T_{e,i\mathrm{MS}} \pm eu_dA_x/T_{e,i\mathrm{MS}})\mathrm{erf}(-\varphi/\varphi_0)$, where $T_{e,i\mathrm{MS}}$ are electron and ion temperatures on the magnetosheath side, and factor $\delta > 1$ determines the relative density increase from the plasma sheet side to the magnetosheath

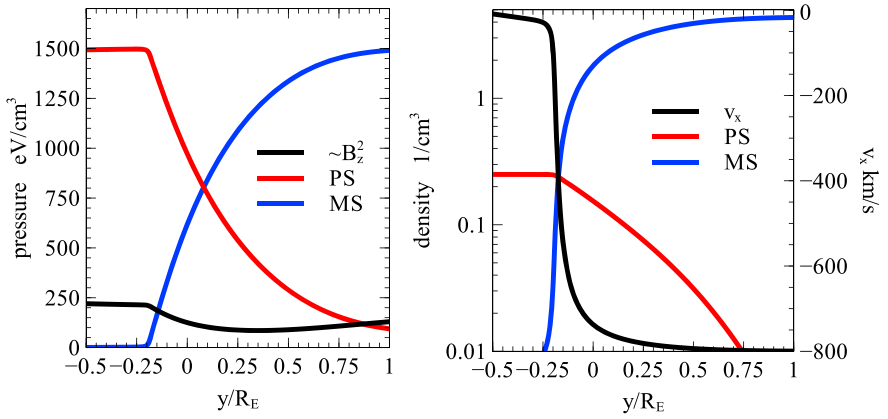

Figure 8. Model distributions of (left) plasma pressure and magnetic field pressure (right) and density and flow velocity for the plasma sheet (PS) and magnetosheath (MS). The magnetic field pressure is shown in Figure 8 (left); the plasma flow velocity is shown in Figure 8 (right). System parameters paraments are $\varphi_0 = 600$ eV, $T_{e,\mathrm{MS}} = 50$ eV, $T_{i,\mathrm{MS}} = 300$ eV, $T_{e,\mathrm{PS}} = 500$ eV, $T_{i,\mathrm{PS}} = 5000$ eV, $u_d = -800$ km/s, and $n_0 = 0.25$ cm^{-3}.

side. The plasma density dependence on the combination of scalar and vector potentials, $\mp e\varphi/T_{e,i\mathrm{MS}} \pm eu_dA_x/T_{e,i\mathrm{MS}}$, shows that the plasma (both ions and electrons) is flowing with velocity $u_d = E_y/B_z$ caused by the quasi-neutrality solution $\varphi = u_dA_x$ for $\varphi \to -\infty$ (see, e.g., discussion in Yoon & Lui, 2004). The factor $\sim \mathrm{erf}(-\varphi/\varphi_0)$ describes the magnetosheath plasma density decrease on the plasma sheet side.

To obtain the spatial distribution of the scalar potential φ, one must solve the quasi-neutrality equation: $n_{i,\mathrm{PS}}(\varphi) + n_{i,\mathrm{MS}}(\varphi, A_x) = n_{e,\mathrm{PS}}(\varphi, A_x) + n_{e,\mathrm{MS}}(\varphi, A_x)$. The solution for A_x is provided by the pressure balance conditions $T_{i,\mathrm{PS}}n_{i,\mathrm{PS}} + T_{e,\mathrm{PS}}n_{e,\mathrm{PS}} + T_{i,\mathrm{MS}}n_{i,\mathrm{MS}} + T_{e,\mathrm{PS}}n_{e,\mathrm{PS}} + (dA_x/dy)^2/2\mu_0k_b = \mathrm{const}$ (see section 6 for details). The input parameters of this model are $T_{i,\mathrm{PS}}$, $T_{e,\mathrm{PS}}$, $T_{i,\mathrm{MS}}$, $T_{e,\mathrm{PS}}$, n_0, φ_0, u_d, and $u_{d\mathrm{PS}}$, and the spatial scale is defined self-consistently. The solution of these two equations (quasi-neutrality and pressure balance) exists only for some range of the input parameters (see, e.g., discussions in De Keyser et al., 2013, and Dorville et al., 2015), and we vary φ_0 to find the solution with the smallest spatial scale (as it will be seen from the solutions shown below, this scale appears to have a realistic value).

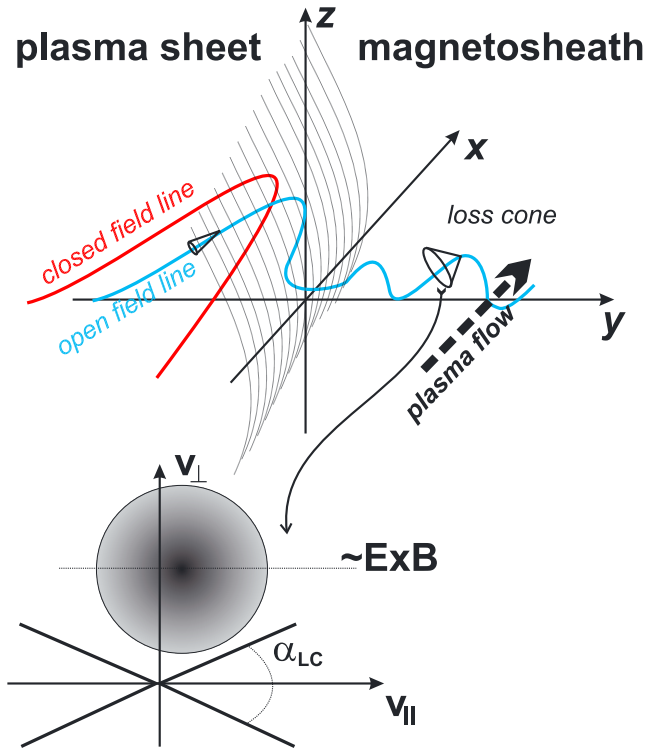

Figure 9. Schematic of ion motion through the boundary layer.

Figures 7 and 8 show two examples of solutions for the boundary layer plasma characteristic distributions (input parameters are indicated in the figure captions). Note that the choice of the y axis origin is arbitrary, so the position of $y = 0$ does not provide any information. The magnetic field pressure is always lower than the plasma pressure (as in the observations). The boundary layer scale (region with a significant overlap between the plasma sheet and magnetosheath plasma densities) is $\sim 1\ R_E$; that is, in the observations a spacecraft would cross this boundary layer for ~2 min with a reasonable velocity along the normal to the boundary surface ~50 km/s. Hot plasma sheet ions penetrate the magnetosheath side deeply. The plasma flow v_x smoothly transitions from an almost uniform profile on the magnetosheath side to a zero value on the plasma sheet side. Therefore, we describe the main characteristics of the observed boundary layer and demonstrate that two different plasmas can be separated by an electrostatic potential drop in the absence of a strong magnetic field gradients.

We construct a series of solutions for a broad range of $u_d \in [-300, -1,000]$ km/s and plasma temperature values. According to these solutions, φ_0 does not depend significantly on the plasma flow amplitude u_d, and it is about $T_{i\mathrm{PS}}$. Therefore, to separate two demagnetized plasmas, we must rely on an electric field potential drop with an amplitude about the energy (temperature) of the hottest plasma component. This potential

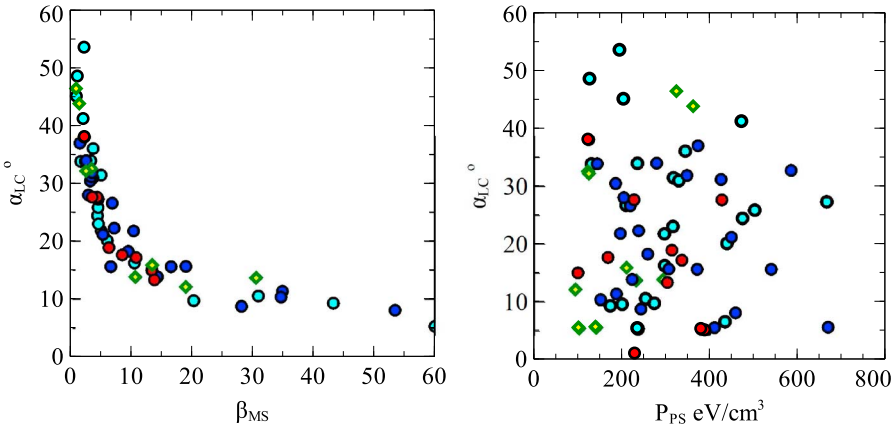

Figure 10. Magnetosheath loss cone size as a function of the (left) magnetosheath β and the (right) plasma sheet total pressure.

drop is generated by the separation of ion and electron motions around the boundary layer. The weak but finite magnetic field B_z plays an important role in generation of the magnetosheath plasma flow $\sim E_y/B_z$.

5. Loss Cone and Magnetosheath Plasma Losses

The lack of a strong magnetic field separating two plasmas at the flank distant magnetotail shows that this separation should be supported by electrostatic fields. However, such separation would take place only in the absence of direct connection between magnetic field lines in the plasma sheet and those in the sides of the magnetosheath sides. Taking into account the fluctuating nature of the magnetosheath field and the significant contribution of the interplanetary magnetic field to boundary layer orientation (e.g., Chen et al., 2015; Sibeck, Siscoe, Slavin, Smith, & Tsurutani, 1985; Sibeck, Siscoe, Slavin, Smith, Tsurutani, & Lepping, 1985), we should assume that magnetic field lines in the plasma sheet are connected to those in the sides of the magnetosheath (at least sometimes). Thus, two types of plasma should be able to cross this boundary layer. If the rarefied plasma sheet plasma were not seen on the magnetosheath side, the dense magnetosheath plasma should be easily detected on the plasma sheet side. Instead, we observe a quite pronounced separation between two plasmas indicating that the penetration mechanisms are ineffective.

Let us consider magnetosheath ion motion in a system with plasma sheet field lines connected to magnetosheath field lines. Figure 9 shows a schematic view of such a system. Magnetosheath ions crossing the boundary layer appear on the plasma sheet side and move along field lines to the magnetotail lobes. Only ions with sufficiently small initial (magnetosheath) pitch angles can stay on the plasma sheet side; large pitch angle ions would be reflected back to the magnetosheath. We can estimate the loss cone size in the magnetosheath side as $\sin^2 \alpha_{LC} = B_{MS}/B_{lobe,\,PS}$, where B_{MS} is the magnetosheath magnetic field and $B_{lobe,\,PS} = \sqrt{B^2 + 2\mu_0(p_i + p_e)}$ is the plasma sheet lobe magnetic field calculated from the pressure balance. The magnetosheath ions with $\alpha < \alpha_{LC}$ can enter the plasma sheet side.

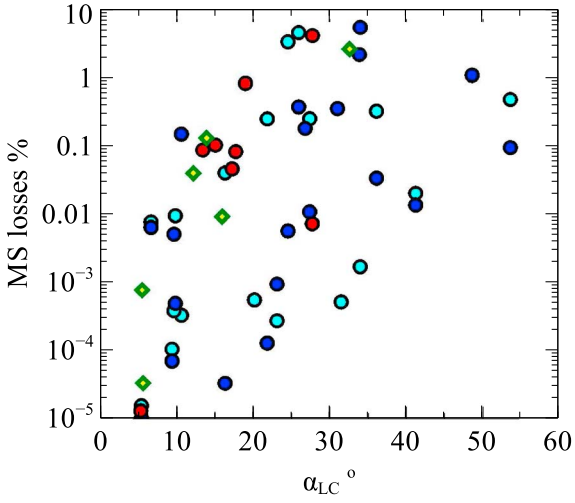

Figure 11. Percentage of the magnetosheath ions occurring within the estimated loss cone.

Figure 10 shows the dependence of α_{LC} on the magnetosheath β and on the total (plasma and magnetic field) pressure on the plasma sheet side. The loss cone size can be quite large (up to 50°); it depends strongly on the magnetosheath β. There is no dependence on the plasma sheet pressure, because the magnetosheath magnetic field variation (from event to event) is much stronger than the variation of the plasma sheet pressure. So a wide loss cone suggests that many magnetosheath ions can enter the plasma sheet side. However, we should take into account that the entire magnetosheath ion distribution is shifted in the velocity space by the cross-field flow v_x (see scheme in Figure 9). This transverse flow removes particles from the loss cone, leaving it empty. To check this assumption, we calculate the percentages of magnetosheath ions within the estimated loss cone.

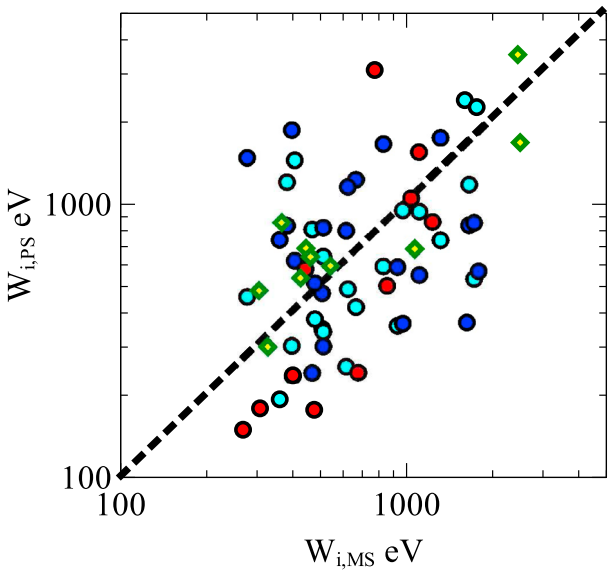

Figure 12. The ion total energy (thermal plus kinetic) in the plasma sheet (PS) and magentosheath (MS).

Figure 11 shows that usually we have losses of less than few percent. This is within the uncertainty of our estimates; that is, we confirm that the magnetosheath loss cone could be wide (in case of magnetic field lines connection) but is empty.

Low-frequency electromagnetic field fluctuations could help transport (scatter) magnetosheath ions into the loss cone (e.g., Chen et al., 2015; Johnson & Cheng, 1997). Such scattered ions would enter the plasma sheet, but the interesting question is can we distinguish these magnetosheath ions in the plasma sheet side? The magnetosheath ion temperature is much lower than the plasma sheet ion temperature; thus, the penetrating ions could be seen as a cold population. However, ion scattering to the loss cone should increase ion thermal energy in cost of the ion kinetic energy. If the pitch angle scattering is due to low-frequency waves, then the total energy (thermal plus kinetic) of scattered ions is conserved (Schulz & Lanzerotti, 1974). Figure 12 compares the total plasma sheet ion energy and total magnetosheath ion energy. These energies are quite similar (or even magnetosheath ions are more energetic for majority of events). Therefore, being scattered into the loss cone (i.e., thermalization without energy loss) and entering to the plasma sheet, the magnetosheath ions would not form a distinct population but would be well mixed with the plasma sheet ions.

6. Discussion

The information about the structure of the distant magnetotail flank discussed in this study allows us to characterize and model plasma motion around the boundary layer and consider possible applications of our results. The data sets used in this study are not exhaustive. Several additional years of ARTEMIS observations (2013–2017) of the lunar distant magnetotail boundary are available, leaving room for more comprehensive statistical investigations. Moreover, the presence of two spacecraft crossing the boundary with some time delay provides additional opportunities for exploring the spatial characteristics of the boundary layer. Another promising yet underutilized approach for further investigation of the magnetotail boundary's response to solar wind conditions is comparison of global MHD results with statistical spacecraft studies (e.g., Sibeck & Lin, 2014). We consider this study, along with the investigations of Chen et al. (2015) and Wang et al. (2014), as a first step in construction of a detailed picture of MHD and kinetic properties of the distant magnetotail boundary layer.

6.1. Plasma Transport Across the Boundary Layer

There is no strong magnetic field around the boundary layer, and both plasma sheet and magnetosheath plasmas are characterized by large β. Comparing our observations with dayside observations (see, e.g., review by De Keyser et al., 2005), we conclude that there is no magnetopause in the distant flank magnetotail, only a boundary layer separating two plasmas. Moreover, fluctuations of the magnetosheath magnetic field open the boundary for direct magnetosheath plasma entry to the plasma sheet side. However, the magnetosheath plasma flow empties the loss cone and significantly reduces the ion population that could move through the boundary layer. Therefore, the most promising mechanism responsible for the magnetosheath plasma transport to the plasma sheet side is particle pitch angle scattering. Several plasma wave modes have been proposed to play an important role in such scattering: low-hybrid drift waves (e.g., Chen et al., 2015), ion cyclotron waves (so far, observed in the dayside magnetopause, see, e.g., Panov et al., 2006), and kinetic Alfvén waves (e.g., Chaston et al., 2013). Effects of all these wave modes have been well studied at the dayside magnetopause, where they heat particles and transport them across the magnetic field (see review by Wing et al., 2014, and references therein). In the distant tail flank, the most important process seems to be pitch angle scattering in a weak magnetic field. This process should resemble the pitch angle scattering of energetic particles traveling through the fluctuating solar wind (e.g., Giacalone & Jokipii, 1999; Sun et al., 2016, and references therein). The approach for calculation of the diffusion rates in such systems is well developed (Jokipii, 1966; Jones et al., 1978) and can be applied for investigation of the ion scattering and transport around the distant magnetotail boundary layer as well.

6.2. Boundary Layer Model Assumptions

We constructed the extremely simple boundary model demonstrating that two demagnetized plasmas can be principally separated by electric fields. However, there is a significant room for improvement of this model to make it more realistic. First of all, we did not provide the reconstructed particle distribution function and thus did not compare kinetics of model and observed plasmas. The well-developed method (Allanson et al., 2016; Channell, 1976) for such reconstruction can be applied to the proposed model in a future study. However, construction of a new model with prescribed particle distributions may be an even more productive approach for describing a realistic boundary layer structure (see examples of such models in Roth et al., 1996). Indeed, for the totally self-consistent description of the plasma equilibrium one needs to derive both plasma density and plasma pressure (or currents). Starting from the plasma density prescription $n(\varphi, A_x)$, we should first reconstruct the distribution function and then derive the pressure distribution $p(\varphi, A_x)$ (for the proposed model estimates we can use the isothermal approximation $T_\gamma = p_\gamma/n_\gamma \approx$ const which can be justified only for large φ_0/T_γ). This is a complicated method with the only one evident advantage: the density profiles can be set initially without choosing the kinetic plasma distributions.

Independently of the chosen method for the construction of the boundary layer model, a more realistic description should include the magnetic field component normal to the boundary layer. Including such a component is not a simple task, because in this case the use of the local integrals of particle motion is not sufficient to describe such boundary layer configuration (see, e.g., discussion in Artemyev, 2011, and Whipple et al., 1984). The possible solution to this problem is to include the adiabatic (approximately conserved) invariants of particle motion (see the corresponding examples in Echim & Lemaire, 2005; Francfort & Pellat, 1976; Sitnov et al., 2000; Zelenyi et al., 2000).

6.3. Possible Applications of Obtained Results

An interesting application of our results on the boundary layer structure is a generalized description of space plasma systems where two demagnetized plasmas are separated. Indeed, boundary layers, together with currents sheets and shock waves, represent a basic element for plasma interactions, that is, for formation of different plasma populations and energy exchange between these populations. Current sheets and shock waves contribute significantly to the magnetic field turbulence in plasma flows, for example, in heliosphere (e.g., Greco et al., 2012; Matthaeus et al., 2015) or pulsar magnetospheres (e.g., Sironi & Spitkovsky, 2011). We can expect that boundary layers with strong density and temperature gradients would contribute to turbulence in demagnetized plasma flows. Such flows can be formed in the boundary of stellar magnetospheres (see, e.g., discussion of the heliotail boundary in McComas et al., 2013). There are several models (both fluid and hybrid) describing of the heliosphere boundary (see, e.g., Izmodenov & Alexashov, 2015; Opher, 2016; Pogorelov et al., 2017, and references therein). Analysis and adaptation of data collected by ARTEMIS observations of the distant Earth magnetotail boundary may help to verify physical mechanisms responsible for the heliosphere boundary formation in these models.

7. Conclusions

This study focuses on the structure of the distant magnetotail boundary layer. We use three data sets to investigate this plasma structure at different radial distances. The main conclusions can be summarized as follows:

1. Plasma and magnetic field characteristics are very similar for boundary layers observed at the lunar orbit ($r \sim 55\ R_E$) and farther downtail as far as $r \sim 200\ R_E$. The dynamical magnetosheath pressure does not contribute to the pressure balance across the boundary layer; that is, the boundary surface should be parallel to the magnetosheath plasma flow.
2. The distant magnetotail flanks are characterized by the absence of clear magnetopause signatures. Both plasma sheet and magnetosheath sides are filled by demagnetized (high β) plasmas, that is, without a significant magnetic field and currents (magnetic field gradients).
3. The separation of the plasma sheet and magnetosheath plasmas at the boundary layer is likely due to electrostatic fields. The connection of the plasma sheet and magnetosheath magnetic field lines (if present) cannot result in ion entry to the magnetosphere, because the strong cross-field magnetosheath plasma flow cleans the loss cone.

4. Total energies (kinetic plus thermal) are very close for the plasma sheet and magnetosheath ions. The magnetosheath ion thermalization should result in formation of an ion population that is indistinguishable from the plasma sheet population and most likely a dominant contributor to it.

Acknowledgments
We are thankful to J. Hohl for her assistance with the manuscript editing. This work was supported by NASA grant NNX16AF84G and NASA contract NAS5-02099. Work of C.-P. Wang was supported by NASA NNX16AJ83G. We would like to thank the following people specifically C. W. Carlson and J. P. McFadden for use of ESA data, D. E. Larson for use of SST data, K. H. Glassmeier, U. Auster, and W. Baumjohann for the use of FGM data provided under the lead of the Technical University of Braunschweig and with financial support through the German Ministry for Economy and Technology and the German Aerospace Center (DLR) under contract 50 OC 0302. All data were downloaded from http://themis.ssl.berkeley.edu/ and http://cdaweb.gsfc.nasa.gov/.

References

Allanson, O., Neukirch, T., Troscheit, S., & Wilson, F. (2016). From one-dimensional fields to Vlasov equilibria: Theory and application of Hermite polynomials. *Journal of Plasma Physics*, *82*(3), 905820306. https://doi.org/10.1017/S0022377816000519

Allanson, O., Neukirch, T., Wilson, F., & Troscheit, S. (2015). An exact collisionless equilibrium for the Force-Free Harris Sheet with low plasma beta. *Physics of Plasmas*, *22*(10), 102116. https://doi.org/10.1063/1.4934611

Alpers, W. (1969). Steady state charge neutral models of the magnetopause. *Astrophysics and Space Science*, *5*, 425–437.

Alpers, W. (1971). On the equilibrium of an exact charge neutral magnetopause. *Astrophysics and Space Science*, *11*, 471–474. https://doi.org/10.1007/BF00649640

Angelopoulos, V. (2011). The ARTEMIS mission. *Space Science Reviews*, *165*, 3–25. https://doi.org/10.1007/s11214-010-9687-2

Artemyev, A. V. (2011). A model of one-dimensional current sheet with parallel currents and normal component of magnetic field. *Physics of Plasmas*, *18*(2), 022104. https://doi.org/10.1063/1.3552141

Artemyev, A. V., Angelopoulos, V., Runov, A., & Vasko, I. Y. (2017). Hot ion flows originating from the distant X-line: ARTEMIS observations from lunar orbit to $x \sim -200\,R_E$. *Journal of Geophysical Research: Space Physics*, *122*. https://doi.org/10.1002/2017JA024433

Auster, H. U., Glassmeier, K. H., Magnes, W., Aydogar, O., Baumjohann, W., Constantinescu, D., … Wiedemann, M. (2008). The THEMIS fluxgate magnetometer. *Space Science Reviews*, *141*, 235–264. https://doi.org/10.1007/s11214-008-9365-9

Belmont, G., Aunai, N., & Smets, R. (2012). Kinetic equilibrium for an asymmetric tangential layer. *Physics of Plasmas*, *19*(2), 022108. https://doi.org/10.1063/1.3685707

Channell, P. J. (1976). Exact Vlasov-Maxwell equilibria with sheared magnetic fields. *Physics of Fluids*, *19*, 1541–1545. https://doi.org/10.1063/1.861357

Chaston, C. C., Yao, Y., Lin, N., Salem, C., & Ueno, G. (2013). Ion heating by broadband electromagnetic waves in the magnetosheath and across the magnetopause. *Journal of Geophysical Research: Space Physics*, *118*, 5579–5591. https://doi.org/10.1002/jgra.50506

Chen, S.-H., Le, G., & Fok, M.-C. (2015). Magnetospheric boundary perturbations on MHD and kinetic scales. *Journal of Geophysical Research: Space Physics*, *120*, 113–137. https://doi.org/10.1002/2014JA020141

Chen, S.-H., Kivelson, M. G., Gosling, J. T., Walker, R. J., & Lazarus, A. J. (1993). Anomalous aspects of magnetosheath flow and of the shape and oscillations of the magnetopause during an interval of strongly northward interplanetary magnetic field. *Journal of Geophysical Research*, *98*, 5727–5742. https://doi.org/10.1029/92JA02263

De Keyser, J., & Roth, M. (1998). Equilibrium conditions and magnetic field rotation at the tangential discontinuity magnetopause. *Journal of Geophysical Research*, *103*, 6653–6662. https://doi.org/10.1029/97JA03710

De Keyser, J., & Roth, M. (2003). Structural analysis of periodic surface waves on the magnetospheric boundary. *Planetary Space Science*, *51*, 757–768. https://doi.org/10.1016/S0032-0633(03)00112-0

De Keyser, J., Dunlop, M. W., Owen, C. J., Sonnerup, B. U. Ö., Haaland, S. E., Vaivads, A., … Rezeau, L. (2005). Magnetopause and boundary layer. *Space Science Reviews*, *118*, 231–320. https://doi.org/10.1007/s11214-005-3834-1

De Keyser, J., Echim, M., & Roth, M. (2013). Cross-field flow and electric potential in a plasma slab. *Annales Geophysicae*, *31*, 1297–1314. https://doi.org/10.5194/angeo-31-1297-2013

De Keyser, J., Gustafsson, G., Roth, M., Darrouzet, F., Dunlop, M., Rème, H., … Cornilleau-Wehrlin, N. (2004). Reconstruction of the magnetopause and low-latitude boundary layer topology using Cluster multi-point measurements. *Annales Geophysicae*, *22*, 2381–2389. https://doi.org/10.5194/angeo-22-2381-2004

Dimmock, A. P., & Nykyri, K. (2013). The statistical mapping of magnetosheath plasma properties based on THEMIS measurements in the magnetosheath interplanetary medium reference frame. *Journal of Geophysical Research: Space Physics*, *118*, 4963–4976. https://doi.org/10.1002/jgra.50465

Dorville, N., Belmont, G., Aunai, N., Dargent, J., & Rezeau, L. (2015). Asymmetric kinetic equilibria: Generalization of the BAS model for rotating magnetic profile and non-zero electric field. *Physics of Plasmas*, *22*(9), 092904. https://doi.org/10.1063/1.4930210

Dungey, J. W. (1963). Interactions of solar plasma with the geomagnetic field. *Planetary Space Science*, *10*, 233–237. https://doi.org/10.1016/0032-0633(63)90020-5

Echim, M. M., & Lemaire, J. F. (2005). Two-dimensional Vlasov solution for a collisionless plasma jet across transverse magnetic field lines with a sheared bulk velocity. *Physical Review E*, *72*(3), 036405. https://doi.org/10.1103/PhysRevE.72.036405

Erkaev, N. V., Farrugia, C. J., Harris, B., & Biernat, H. K. (2011). On accelerated magnetosheath flows under northward IMF. *Geophysical Research Letters*, *38*, L01104. https://doi.org/10.1029/2010GL045998

Fairfield, D. H., Otto, A., Mukai, T., Kokubun, S., Lepping, R. P., Steinberg, J. T., … Yamamoto, T. (2000). Geotail observations of the Kelvin-Helmholtz instability at the equatorial magnetotail boundary for parallel northward fields. *Journal of Geophysical Research*, *105*, 21,159–21,173. https://doi.org/10.1029/1999JA000316

Francfort, P., & Pellat, R. (1976). Magnetic merging in collisionless plasmas. *Geophysical Research Letters*, *3*, 433–436. https://doi.org/10.1029/GL003i008p00433

Fujimoto, M., Mukai, T., Kawano, H., Nakamura, M., Nishida, A., … Kokubun, S. (1997). A Geotail observation of low-latitude boundary layer. *Advances in Space Research*, *20*, 813–822. https://doi.org/10.1016/S0273-1177(97)00514-0

Fujimoto, M., Terasawa, T., Mukai, T., Saito, Y., Yamamoto, T., & Kokubun, S. (1998). Plasma entry from the flanks of the near-Earth magnetotail: Geotail observations. *Journal of Geophysical Research*, *103*, 4391–4408. https://doi.org/10.1029/97JA03340

Galeev, A. A., Kuznetsova, M. M., & Zelenyi, L. M. (1986). Magnetopause stability threshold for patchy reconnection. *Space Science Reviews*, *44*, 1–41. https://doi.org/10.1007/BF00227227

Giacalone, J., & Jokipii, J. R. (1999). The transport of cosmic rays across a turbulent magnetic field. *Astrophysics Journal*, *520*, 204–214. https://doi.org/10.1086/307452

Grad, H. (1961). Boundary layer between a plasma and a magnetic field. *Physics of Fluids*, *4*, 1366–1375. https://doi.org/10.1063/1.1706226

Greco, A., Matthaeus, W. H., D'Amicis, R., Servidio, S., & Dmitruk, P. (2012). Evidence for nonlinear development of magnetohydrodynamic scale intermittency in the inner heliosphere. *Astrophysics Journal*, *749*, 105. https://doi.org/10.1088/0004-637X/749/2/105

Grzedzielski, S., & Macek, W. (1988). An open magnetopause model of the Earth's distant tail based on ISEE 3 evidence. *Journal of Geophysical Research*, *93*, 1795–1808. https://doi.org/10.1029/JA093iA03p01795

Haaland, S., Paschmann, G., Förster, M., Quinn, J., Torbert, R., Vaith, H., … Kletzing, C. (2008). Plasma convection in the magnetotail lobes: Statistical results from Cluster EDI measurements. *Annales Geophysicae*, *26*, 2371–2382. https://doi.org/10.5194/angeo-26-2371-2008

Haaland, S., Reistad, J., Tenfjord, P., Gjerloev, J., Maes, L., DeKeyser, J., … Dorville, N. (2014). Characteristics of the flank magnetopause: Cluster observations. *Journal of Geophysical Research: Space Physics*, *119*, 9019–9037. https://doi.org/10.1002/2014JA020539

Harris, E (1962). On a plasma sheet separating regions of oppositely directed magnetic field. *Nuovo Cimento*, *23*, 115–123.

Harris, B., Farrugia, C. J., Erkaev, N. V., & Torbert, R. B. (2013). Observational aspects of IMF draping-related magnetosheath accelerations for northward IMF. *Annales Geophysicae*, *31*, 1779–1789. https://doi.org/10.5194/angeo-31-1779-2013

Hasegawa, H., Fujimoto, M., Phan, T.-D., Rème, H., Balogh, A., & Dunlop, M. W. (2004). Transport of solar wind into Earth's magnetosphere through rolled-up Kelvin-Helmholtz vortices. *Nature*, *430*, 755–758. https://doi.org/10.1038/nature02799

Hasegawa, H., Maezawa, K., Mukai, T., & Saito, Y. (2002). Plasma entry across the distant tail magnetopause 1. Global properties and IMF dependence. *Journal of Geophysical Research*, *107*, 1063. https://doi.org/10.1029/2001JA900139

Hasegawa, H., Maezawa, K., Saito, Y., Mukai, T., & Kokubun, S. (2000). Dependence of the Distant Tail Magnetopause Position on the Solar Wind and IMF. *Advances in Space Research*, *25*, 1485–1488. https://doi.org/10.1016/S0273-1177(99)00659-6

Hietala, H., Artemyev, A. V., & Angelopoulos, V. (2017). Ion dynamics in magnetotail reconnection in the presence of density asymmetry. *Journal of Geophysical Research: Space Physics*, *122*, 2010–2023. https://doi.org/10.1002/2016JA023651

Izmodenov, V. V., & Alexashov, D. B. (2015). Three-dimensional kinetic-MHD model of the global heliosphere with the heliopause-surface fitting. *The Astrophysical Journal Supplement Series*, *220*, 32. https://doi.org/10.1088/0067-0049/220/2/32

Johnson, J. R., & Cheng, C. Z. (1997). Kinetic Alfvén waves and plasma transport at the magnetopause. *Geophysical Research Letters*, *24*, 1423–1426. https://doi.org/10.1029/97GL01333

Jokipii, J. R. (1966). Cosmic-ray propagation. I. Charged particles in a random magnetic field. *Astrophysics Journal*, *146*, 480. https://doi.org/10.1086/148912

Jones, F. C., Birmingham, T. J., & Kaiser, T. B. (1978). Partially averaged field approach to cosmic ray diffusion. *Physics of Fluids*, *21*, 347–360. https://doi.org/10.1063/1.862233

Kokubun, S., Yamamoto, T., Acuna, M. H., Hayashi, K., Shiokawa, K., & Kawano, H. (1994). The Geotail magnetic field experiment. *Journal of Geomagnetism and Geoelectricity*, *46*, 7–21.

Lavraud, B., Borovsky, J. E., Ridley, A. J., Pogue, E. W., Thomsen, M. F., & Rème, H. (2007). Strong bulk plasma acceleration in Earth's magnetosheath: A magnetic slingshot effect? *Geophysical Research Letters*, *34*, L14102. https://doi.org/10.1029/2007GL030024

Lee, L. C., & Kan, J. R. (1979). A unified kinetic model of the tangential magnetopause structure. *Journal of Geophysical Research*, *84*, 6417–6426. https://doi.org/10.1029/JA084iA11p06417

Lemaire, J., & Burlaga, L. F. (1976). Diamagnetic boundary layers—A kinetic theory. *Astrophysics and Space Science*, *45*, 303–325. https://doi.org/10.1007/BF00642667

Matthaeus, W. H., Wan, M., Servidio, S., Greco, A., Osman, K. T., Oughton, S., & Dmitruk, P. (2015). Intermittency, nonlinear dynamics and dissipation in the solar wind and astrophysical plasmas. *Philosophical Transactions of the Royal Society of London A: Mathematical, Physical and Engineering Sciences*, *373*, 20140154. https://doi.org/10.1098/rsta.2014.0154

McComas, D. J., Dayeh, M. A., Funsten, H. O., Livadiotis, G., & Schwadron, N. A. (2013). The heliotail revealed by the interstellar boundary explorer. *Astrophysics Journal*, *771*, 77. https://doi.org/10.1088/0004-637X/771/2/77

McFadden, J. P., Carlson, C. W., Larson, D., Ludlam, M., Abiad, R., & Elliott, B. (2008). The THEMIS ESA plasma instrument and in-flight calibration. *Space Science Reviews*, *141*, 277–302. https://doi.org/10.1007/s11214-008-9440-2

Mukai, T., Machida, S., Saito, Y., Hirahara, M., Terasawa, T., Kaya, N., … Nishida, A. (1994). The low energy particles (LEP) experiment onboard the Geotail satellite. *Journal of Geomagnetism and Geoelectricity*, *46*, 669–692.

Nakai, H., & Ueno, G. (2011). Plasma structures of Kelvin-Helmholtz billows at the duskside flank of the magnetotail. *Journal of Geophysical Research*, *116*, A08212. https://doi.org/10.1029/2010JA016286

Nishida, A. (1994). The GEOTAIL mission. *Geophysical Research Letters*, *21*, 2871–2873. https://doi.org/10.1029/94GL01223

Ogilvie, K. W., von Rosenvinge, T., & Durney, A. C. (1977). International Sun-Earth Explorer: A three-spacecraft program. *Science*, *198*, 131–138. https://doi.org/10.1126/science.198.4313.131

Opher, M. (2016). The heliosphere: What did we learn in recent years and the current challenges. *Space Science Reviews*, *200*, 475–494. https://doi.org/10.1007/s11214-015-0186-3

Panov, E. V., Artemyev, A. V., Nakamura, R., & Baumjohann, W. (2011). Two types of tangential magnetopause current sheets: Cluster observations and theory. *Journal of Geophysical Research*, *116*, A1204. https://doi.org/10.1029/2011JA016860

Panov, E. V., Büchner, J., Fränz, M., Korth, A., Savin, S. P., & Fornaçon, K.-H. (2006). CLUSTER observation of collisionless transport at the magnetopause. *Geophysical Research Letters*, *33*, L15109. https://doi.org/10.1029/2006GL026556

Panov, E. V., Büchner, J., Fränz, M., Korth, A., Savin, S. P., Rème, H., & Fornaçon, K. (2008). High-latitude Earth's magnetopause outside the cusp: Cluster observations. *Journal of Geophysical Research*, *113*, 1220. https://doi.org/10.1029/2006JA012123

Peroomian, V. (2003). Interplanetary magnetic field-dependent impact of solar wind ions on Earth's magnetopause. In *Earth's low-latitude boundary layer, Geophysical Monograph Series* (Vol. 133, pp. 45–52). Washington, DC: American Geophysical Union. https://doi.org/10.1029/133GM04

Peroomian, V., & El-Alaoui, M. (2008). The storm-time access of solar wind ions to the nightside ring current and plasma sheet. *Journal of Geophysical Research*, *113*, A06215. https://doi.org/10.1029/2007JA012872

Phan, T. D. (1997). Low-latitude dusk flank magnetosheath, magnetopause, and boundary layer for low magnetic shear: Wind observations. *Journal of Geophysical Research*, *102*, 19,883–19,896. https://doi.org/10.1029/97JA01596

Phan, T. D., & Paschmann, G. (1996). Low-latitude dayside magnetopause and boundary layer for high magnetic shear 1. Structure and motion. *Journal of Geophysical Research*, *101*, 7801–7816. https://doi.org/10.1029/95JA03752

Plaschke, F. (2016). *ULF waves at the magnetopause, Geophysical Monograph Series* (Vol. 216, pp. 193–212). Washington, DC: American Geophysical Union. https://doi.org/10.1002/9781119055006.ch12

Pogorelov, N. V., Fichtner, H., Czechowski, A., Lazarian, A., Lembege, B., le Roux, J. A., … Zhang, M. (2017). Heliosheath processes and the structure of the heliopause: Modeling energetic particles, cosmic rays, and magnetic fields. *Space Science Reviews*, *212*, 193. https://doi.org/10.1007/s11214-017-0354-8

Roth, M., de Keyser, J., & Kuznetsova, M. M. (1996). Vlasov theory of the equilibrium structure of tangential discontinuities in space plasmas. *Space Science Reviews*, *76*, 251–317. https://doi.org/10.1007/BF00197842

Sanchez, E. R., Siscoe, G. L., & Summers, D. (1990). Downstream evolution of an open MHD magnetotail boundary. *Journal of Geophysical Research*, *95*, 20,743–20,758. https://doi.org/10.1029/JA095iA12p20743

Schulz, M., & Lanzerotti, L. J. (1974). *Particle diffusion in the radiation belts*. New York: Springer.

Sibeck, D. G., & Lin, R.-Q. (2014). Size and shape of the distant magnetotail. *Journal of Geophysical Research: Space Physics*, *119*, 1028–1043. https://doi.org/10.1002/2013JA019471

Sibeck, D. G., Lepping, R. P., & Lazarus, A. J. (1990). Magnetic field line draping in the plasma depletion layer. *Journal of Geophysical Research*, *95*, 2433–2440. https://doi.org/10.1029/JA095iA03p02433

Sibeck, D. G., Siscoe, G. L., Slavin, J. A., Smith, E. J., & Tsurutani, B. T. (1985). Magnetic field properties of the distant magnetotail magnetopause and boundary layer. *Journal of Geophysical Research*, *90*, 9561–9575. https://doi.org/10.1029/JA090iA10p09561

Sibeck, D. G., Siscoe, G. L., Slavin, J. A., Smith, E. J., Tsurutani, B. T., & Lepping, R. P. (1985). The distant magnetotail's response to a strong interplanetary magnetic field B_y—Twisting, flattening, and field line bending. *Journal of Geophysical Research*, *90*, 4011–4019. https://doi.org/10.1029/JA090iA05p04011

Sironi, L., & Spitkovsky, A. (2011). Acceleration of particles at the termination shock of a relativistic striped wind. *Astrophysics Journal*, *741*, 39. https://doi.org/10.1088/0004-637X/741/1/39

Sitnov, M. I., Zelenyi, L. M., Malova, H. V., & Sharma, A. S. (2000). Thin current sheet embedded within a thicker plasma sheet: Self-consistent kinetic theory. *Journal of Geophysical Research*, *105*, 13,029–13,044. https://doi.org/10.1029/1999JA000431

Sun, P., Jokipii, J. R., & Giacalone, J. (2016). Pitch-angle scattering of energetic charged particles in nearly constant magnitude magnetic turbulence. *Astrophysics Journal*, *827*, 16. https://doi.org/10.3847/0004-637X/827/1/16

Treumann, R. A. (1999). Wave turbulence in the plasma sheet and low latitude boundary layers. *Advances in Space Research*, *24*, 3–12. https://doi.org/10.1016/S0273-1177(99)00416-0

Šafránková, J., Němeček, Z., Přech, L., Šimunek, J., Sibeck, D., & Sauvaud, J.-A. (2007). Variations of the flank LLBL thickness as response to the solar wind dynamic pressure and IMF orientation. *Journal of Geophysical Research*, *112*, A07201. https://doi.org/10.1029/2006JA011889

Vasko, I. Y., Petrukovich, A. A., Artemyev, A. V., Nakamura, R., & Zelenyi, L. M. (2015). Earth's distant magnetotail current sheet near and beyond lunar orbit. *Journal of Geophysical Research: Space Physics*, *120*, 8663–8680. https://doi.org/10.1002/2015JA021633

Wang, C.-P., Lyons, L. R., & Angelopoulos, V. (2014). Properties of low-latitude mantle plasma in the Earth's magnetotail: ARTEMIS observations and global MHD predictions. *Journal of Geophysical Research: Space Physics*, *119*, 7264–7280. https://doi.org/10.1002/2014JA020060

Wang, C.-P., Xing, X., Nakamura, T. K. M., Lyons, L. R., & Angelopoulos, V. (2014). Source and structure of bursty hot electron enhancements in the tail magnetosheath: Simultaneous two-probe observation by ARTEMIS. *Journal of Geophysical Research: Space Physics*, *119*, 9900–9918. https://doi.org/10.1002/2014JA020603

Whipple, E. C., Hill, J. R., & Nichols, J. D. (1984). Magnetopause structure and the question of particle accessibility. *Journal of Geophysical Research*, *89*, 1508–1516. https://doi.org/10.1029/JA089iA03p01508

Wing, S., Johnson, J. R., Chaston, C. C., Echim, M., Escoubet, C. P., Lavraud, B., … Wang, C.-P. (2014). Review of solar wind entry into and transport within the plasma sheet. *Space Science Reviews*, *184*, 33–86. https://doi.org/10.1007/s11214-014-0108-9

Yoon, P. H., & Lui, A. T. Y. (2004). Model of ion- or electron-dominated current sheet. *Journal of Geophysical Research*, *109*, A11213. https://doi.org/10.1029/2004JA010555.

Zelenyi, L. M., Sitnov, M. I., Malova, H. V., & Sharma, A. S. (2000). Thin and superthin ion current sheets. Quasi-adiabatic and nonadiabatic models. *Nonlinear Processes in Geophysics*, *7*, 127–139.